PHYSICAL REVIEW D VOLUME 22, NUMBER 1 1 JULY 1980

Ghost-pole subtraction and the σ-exchange NN potential

Earle L. Lomon
Center for Theoretical Physics, Laboratory for Nuclear Science and Department of Physics, Massachusetts Institute of Technology, Cambridge, Massachusetts 02139
(Received 5 December 1979)

The summing of all pion bubble graphs in the computation of the σ-meson propagator leads to the appearance of ghost poles when $\sigma\pi\pi$ coupling strengths are equivalent to σ-meson decay widths greater than 625.2 MeV. A result satisfying dispersion relations is obtained by the direct subtraction of the ghost pole from the results published previously by this author. The effect is to decrease the sensitivity to the σ-meson width of both the central and spin-orbit nucleon-nucleon potentials. The potentials are small for separations greater than half a pion Compton wavelength and decrease in magnitude with increasing width. Larger widths are more compatible with phenomenological and dispersion-theory potentials.

I. INTRODUCTION

In Ref. 1 (hereafter referred to as L1), the contribution to the nucleon-nucleon potential of the infinite set of graphs indicated by Fig. 1 was computed. These are all graphs consisting of a single σ-meson exchange but allowing the σ meson to decay into two pions and recombine any number of times. It includes diagrams in which either the σ meson or two pions are attached to each nucleon line.

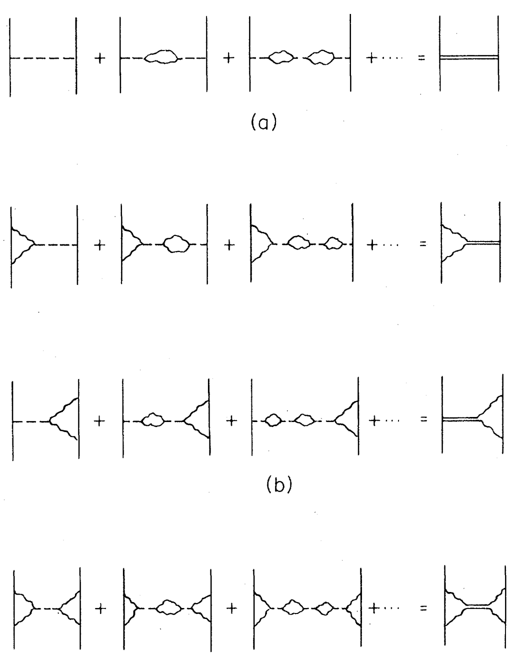

FIG. 1. σ-meson-exchange contributions to the nucleon-nucleon interaction including any number of decays into 2 pions. The use of the modified propagator enables all the graphs to be represented by four graphs. (a) $^{\Gamma}V^{\sigma}$, (b) $^{\Gamma}V^{\sigma\pi}$, (c) $^{\Gamma}V^{\sigma\pi\pi}$.

The summation of each infinite set of graphs consisting of any number of pion bubble insertions on a σ-meson line, leads, for each set of graphs to the replacement of the free σ-meson propagator $G_\sigma(q^2)=[q^2-(M_\sigma^0)^2]^{-1}$ by a modified propagator $\bar{G}_\sigma(q^2)$. The properties of $\bar{G}_\sigma(q^2)$ were extensively discussed in L1, including the appearance of a pole on the real q^2 axis at $q^2<4\mu^2$ for very large widths of σ decay into two pions, $\Gamma_\sigma>\Gamma_\sigma^{\text{crit}}$ (M_σ^0 is the bare σ-meson mass, μ is the pion mass, Γ_σ is the σ-meson width, and q^2 is the virtual barycentric mass of the σ meson and is also the square of the four-momentum transfer between the nucleons. We use units in which $\hbar=c=1$). This pole was interpreted in L1 as the appearance of an unobserved bound state of the two-pion system when the pole q_p^2 satisfied $0<q_p^2<4\mu^2$. When $q_p^2<0$, a real pole appears in the NN amplitude which has no physical interpretation. The NN potentials arising from cases with $\Gamma_\sigma>\Gamma_\sigma^{\text{crit}}$ were presented but not accepted as meaningful.

It was pointed out[2] to the author that the real poles in $\bar{G}_\sigma(q^2)$ were in fact "ghost" poles. Redmond[3] has shown that if the required analytical properties are imposed, through a dispersion relation, on such a propagator, the answer is equivalent to subtracting the ghost pole from the summed perturbation series. The correct results corresponding to the infinite series of graphs can be recovered from the singular perturbation result by locating the position of the ghost pole, calculating its residue, and subtracting the pole from the perturbation-sum result. This corresponds to adding a term whose formal expansion in powers of the coupling constant has vanishing coefficients.[3]

In this paper the conditions for the appearance of the ghost pole, its location, and its residue are described. The ghost-free modified propagator $\hat{G}_\sigma$ is then applied to calculating the poten-

 © 1980 The American Physical Society

tial for two cases of physical interest. The two cases correspond to the large widths predicted by the original σ model of Gell-Mann and Lévy[4] with $g_A/g_v = 1.37$ or 1.0. The smaller width corresponding to the Weinberg model[5] is very nearly the width for which the residue of the ghost pole vanishes. Hence, the potential for that case remains the same as the result given in L1.

II. THE POSITION AND RESIDUE OF THE GHOST POLE

The sum of all bubble graphs indicated in Fig. 2 is easily obtained by summing a geometric series based on the primitive graph with one bubble. The result is [the content of Eqs. (9), (11), (14), and (15) of L1 is repeated below in a more convenient form for easy reference]

$$\bar{G}_\sigma^{-1}(q^2) = q^2 - M_\sigma^{\,2} - \bar{I}_B(q^2) + \mathrm{Re}\bar{I}_B(M_\sigma^{\,2})\,, \tag{1}$$

where M_σ is the physical σ-meson mass and

$$\bar{I}_B(q^2) = \pi^2\lambda_B(-2 + 2Q\tanh^{-1}Q^{-1})\,, \quad q^2 < 4\mu^2 \tag{2a}$$

$$\bar{I}_B(q^2) = \pi^2\lambda_B(-2 + 2Q\tanh^{-1}Q - i\pi Q)\,, \quad q^2 > 0 \tag{2b}$$

with

$$Q = (1 - 4\mu^2 q^{-2})^{1/2}\,, \quad \lambda_B = 6(2\pi)^{-4} g_{\sigma\pi}^{\;2}\,,$$

and

$$-\pi/2 \le \tan^{-1}\theta < \pi/2 \text{ for imaginary } Q\,.$$

The $\mathrm{Re}[\bar{G}_\sigma^{-1}(q^2)]$ vanishes when $q^2 = M_\sigma^{\,2}$ indicating that, as $M_\sigma^{\,2} > 4\mu^2$, there is a nearby pole off the real axis on an unphysical sheet. This is, of course, the Breit-Wigner-type pole responsible for the σ-meson resonance. The $\mathrm{Im}[I_B(q^2)] < 0$ for $q^2 > 4\mu^2$ and determines the decay width

$$\Gamma_\sigma = \pi^3\lambda_B M_\sigma^{\,-1}(1 - 4\mu^2 M_\sigma^{\,-2})^{1/2}\,, \tag{3}$$

and the correct two-pion S-wave threshold behavior is given by the factor Q. As Γ_σ increases, this pole moves further away from the physical sheet.

We now examine the conditions for the appearance of a pole, distinct from the Breit-Wigner pole, on the physical sheet. The function $\pi^{-2}\lambda_B^{\,-1}\mathrm{Re}\bar{I}_B(q^2) \equiv J(q^2)$ is independent of λ_B. It has a minimum value of -2 at $q^2 = 4\mu^2$ where it has a zeroth-order cusp. This is shown in Fig. 3 from which it is also evident that for $\lambda_B > \lambda_B^{\mathrm{crit}}$ determined

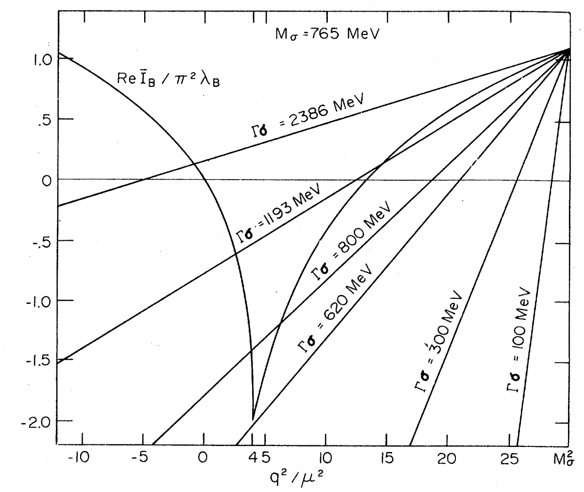

FIG. 3. The linear and nonlinear terms of $\mathrm{Re}[\bar{G}_\sigma^{-1}(q^2)]$ as in Eq. (1). The straight lines represent, with $M_\sigma = 765$ MeV, $(\pi^2\lambda_B)^{-1}(q^2 - M_\sigma^{\,2}) + J(M_\sigma^{\,2})$. The curve is $J(q^2)$. λ_B is proportional to Γ_σ. Intersections represent zeros of $\mathrm{Re}[\bar{G}_\sigma^{-1}(q^2)]$.

by

$$M_\sigma^{\,2} - 4\mu^2 = \pi^2\lambda_B^{\mathrm{crit}}[2 + J(M_\sigma^{\,2})]\,, \tag{4}$$

there are two non-Breit-Wigner zeros of $\mathrm{Re}[\bar{G}_\sigma^{-1}(q^2)]$. Furthermore, one of the zeros has $q^2 > 4\mu$ and the other $q^2 < 4\mu^2$. For $q^2 < 4\mu^2$, the $\mathrm{Im}[\bar{G}_\sigma^{-1}] = 0$ and we obtain a real root. This root is a ghost as it is on the physical sheet and must be subtracted. For $M_\sigma = 765$ MeV, $\Gamma_\sigma^{\mathrm{crit}} = 625.2$ MeV [corresponding to $\lambda_B = \lambda_B^{\mathrm{crit}}$ in Eq. (3)]. For $\lambda_B < \lambda_B^{\mathrm{crit}}$, the pole moves onto the unphysical sheet corresponding to $Q = -(1 - 4\mu^2 q^{-2})^{1/2}$ and moves back along the real q^2 axis.

The zero of $\mathrm{Re}[\bar{G}_\sigma^{-1}(q^2)]$ for $q^2 > 4\mu^2$, when $\lambda_B > \lambda_B^{\mathrm{crit}}$, is not close to a pole of $\bar{G}_\sigma(q^2)$ because of $\mathrm{Im}[\bar{G}_\sigma^{-1}(q^2)]$. The latter vanishes as $(q^2 - 4\mu^2)^{1/2}$ at $q^2 = 4\mu^2$, which is of the same order as the distance of the zero of $\mathrm{Re}[\bar{G}_\sigma^{-1}(q^2)]$ from the branch point. The result is that no value of q^2 in the vicinity satisfies $\bar{G}_\sigma^{-1}(q^2) = 0$. Calculations indicate that the remaining poles of the propagator are at distances greater than $4\mu^2$ from $q^2 = 4\mu^2$ and are on unphysical sheets reached through the cut whose branch point is at $q^2 = 0$. A similar situation exists for this pole when $\lambda_B < \lambda_B^{\mathrm{crit}}$. It follows that one ghost pole exists only for

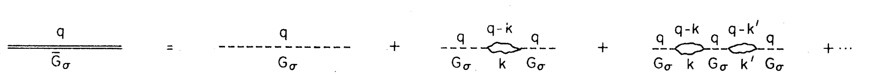

FIG. 2. The modified σ-meson propagator $\bar{G}_\sigma$ obtained by summing graphs of the bare propagator G_σ with any number of pion bubble insertions. $\hat{G}_\sigma$ is obtained from $\bar{G}_\sigma$ by subtraction of the ghost pole.

$\lambda_B > \lambda_B^{\rm crit}$ and it is on the real q^2 axis, $q^2 \leqslant 4\mu^2$.

Near the pole $\bar{G}_\sigma^{-1}(q^2) = (q^2 - q_p^2)R^{-1}$, where the residue R is given by $(q^2 < 4\mu^2)$,

$$R^{-1} = \left(\frac{d\bar{G}_\sigma^{-1}}{dq^2}\right)_{q^2=q_p^2} = \left(1 - \frac{d\bar{I}_B}{dq^2}\right)_{q^2=q_p^2}$$

$$= 1 - \pi^2\lambda_B q_p^{-2}(1 + 4\mu^2 q_p^{-2} Q_p^{-1}\tanh^{-1}Q_p^{-1}) \quad (5)$$

with $Q_p = Q(q_p^2)$. A more convenient form when $0 < q^2 < 4\mu^2$ is

$$R^{-1} = 1 - \pi^2\lambda_B q_p^{-2}(1 - 4\mu^2 q_p^{-2}|Q_p^{-1}|\tan^{-1}|Q_p^{-1}|)\,. \quad (5')$$

III. RESULTS

It follows from Eq. (5′) that when $q_p^2 = 4\mu^2$, $R = 0$. Therefore, when $\Gamma_\sigma = \Gamma_\sigma^{\rm crit}$, the residue vanishes and a ghost-pole subtraction is not required, leading continuously into the region $\Gamma_\sigma < \Gamma_\sigma^{\rm crit}$ where there are no ghost poles. Therefore, the results of the Weinberg model,[5] for which $\Gamma_\sigma \approx 620$ MeV, remain unchanged from those given in L1.

Analysis of pion-production experiments (see Refs. 4, 6, and 7 of L1) indicates that $600 \lesssim \Gamma_\sigma \lesssim 1200$ MeV. The Gell-Mann–Lévy model[4] with $g_A/g_V = 1.37$ gives $\Gamma_\sigma = 1193$ MeV near the upper end of this range. We will present the results for this case and also for the Gell-Mann–Lévy model with $g_A/g_V = 1$, corresponding to $\Gamma_0 = 2386$ MeV to indicate the asymptotic behavior.

Using Eqs. (1), (2a), (5), and (5′), and $M_\sigma = 765$ MeV one obtains, for $\Gamma_\sigma = 1193$ MeV, $q_p^2 = 2.570\,43\,\mu^2$ and $R = 0.145\,79$; and for $\Gamma_\sigma = 2386$ MeV, $q_p^2 = -0.889\,92$ and $R = 0.180\,56$.

For each value of Γ_σ one obtains

$$\hat{G}_\sigma(q^2) = \bar{G}_\sigma(q^2) - R(q^2 - q_p^2)^{-1} \quad (6)$$

and then computes the contributions to the

TABLE I. The values of the central σ-meson-exchange potentials defined as in L1, but with $\hat{G}_\sigma$ replacing $\bar{G}_\sigma$. $M_\sigma = 765$ MeV, $\Gamma_\sigma = 1193$ MeV.

r ($\hbar/\mu c$)	rV_c^{σ} (μc^2)	$rV_c^{\sigma\pi}$ (μc^2)	$rV_c^{\sigma\pi\pi}$ (μc^2)	$rV_c^{\sigma E}$ (μc^2)
0.4	−31.22	33.14	−7.28	−5.35
0.5	−15.99	18.80	−4.54	−1.73
0.6	−8.84	11.24	−2.93	−0.52
0.7	−5.17	6.99	−1.93	−0.11
0.8	−3.15	4.48	−1.30	0.028
0.9	−1.99	2.94	−0.89	0.064
1.0	−1.29	1.97	−0.62	0.064
1.1	−0.85	1.34	−0.43	0.055
1.2	−0.58	0.93	−0.31	0.044
1.3	−0.40	0.65	−0.22	0.034

TABLE II. The values of the spin-orbit σ-meson-exchange potentials defined as in L1, but with $\hat{G}_\sigma$ replacing $\bar{G}_\sigma$. $M_\sigma = 765$ MeV, $\Gamma_\sigma = 1193$ MeV.

r ($\hbar/\mu c$)	$rV_{\rm so}^{\sigma}$ (μc^2)	$rV_{\rm so}^{\sigma\pi}$ (μc^2)	$rV_{\rm so}^{\sigma\pi\pi}$ (μc^2)	$rV_{\rm so}^{\sigma E}$ (μc^2)
0.4	−7.28	5.69	−0.95	−2.53
0.5	−2.54	2.35	−0.45	−0.65
0.6	−1.03	1.08	−0.23	−0.18
0.7	−0.46	0.53	−0.13	−0.054
0.8	−0.23	0.28	−0.071	−0.015
0.9	−0.12	0.16	−0.042	−0.003
1.0	−0.064	0.089	−0.025	0.0002
1.1	−0.036	0.053	−0.016	0.001
1.2	−0.021	0.032	−0.010	0.0011
1.3	−0.013	0.020	−0.006	0.0009

nucleon-nucleon potentials using Eqs. (24)–(31) of L1 with $\hat{G}_\sigma$ replacing $\bar{G}_\sigma$ in Eqs. (24a)–(24f). When $q_p^2 < 0$, the range of integration in Eqs. (28) and (29) includes the position of the subtracted pole. Care must be taken to avoid integration points in the region of uncertainty of the pole position, or to

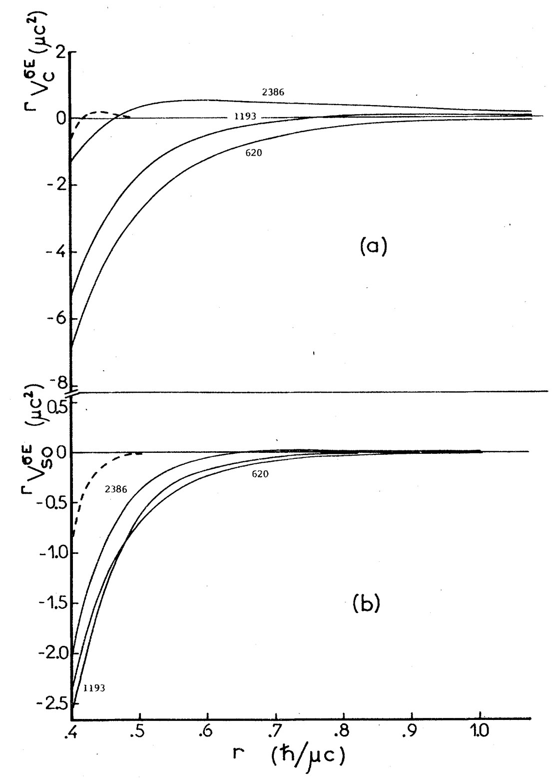

FIG. 4. The total σ-meson-exchange contribution to the nucleon-nucleon interaction. The solid curves are the result of using the ghost-pole-subtracted $\hat{G}_\sigma$ for Γ_σ as marked in MeV. The dashed curve is the result of the ghost-pole-unsubtracted $\bar{G}_\sigma$ for $\Gamma_\sigma = 1193$ MeV. (a) The central potential. (b) The spin-orbit potential.

TABLE III. The values of the central σ-meson-exchange potentials defined as in L1, but with $\hat{G}_\sigma$ replacing $\bar{G}_\sigma$. $M_\sigma = 765$ MeV, $\Gamma_\sigma = 2386$ MeV.

r ($\hbar/\mu c$)	${}^\Gamma V_c^\sigma$ (μc^2)	${}^\Gamma V_c^{\sigma\pi}$ (μc^2)	${}^\Gamma V_c^{\sigma\pi\pi}$ (μc^2)	${}^\Gamma V_c^{\sigma E}$ (μc^2)
0.4	−27.88	34.85	−8.24	−1.28
0.5	−13.66	18.99	−5.02	0.31
0.6	−7.29	10.98	−3.15	0.53
0.7	−4.14	6.68	−2.02	0.52
0.8	−2.46	4.17	−1.33	0.38
0.9	−1.52	2.70	−0.90	0.28
1.0	−0.97	1.77	−0.61	0.19
1.1	−0.63	1.18	−0.43	0.13
1.2	−0.42	0.80	−0.30	0.089

TABLE IV. The values of the spin-orbit σ-meson-exchange potentials defined as in L1, but with $\hat{G}_\sigma$ replacing $\bar{G}_\sigma$. $M_\sigma = 765$ MeV, $\Gamma_\sigma = 2386$ MeV.

r ($\hbar/\mu c$)	${}^\Gamma V_{so}^\sigma$ (μc^2)	${}^\Gamma V_{so}^{\sigma\pi}$ (μc^2)	${}^\Gamma V_{so}^{\sigma\pi\pi}$ (μc^2)	${}^\Gamma V_{so}^{\sigma E}$ (μc^2)
0.4	−7.54	6.70	−1.20	−2.03
0.5	−2.43	2.61	−0.55	−0.37
0.6	−0.93	1.14	−0.27	−0.056
0.7	−0.40	0.54	−0.14	0.005
0.8	−0.19	0.28	−0.077	0.013
0.9	−0.094	0.150	−0.044	0.011
1.0	−0.050	0.084	−0.026	0.008
1.1	−0.028	0.049	−0.016	0.005
1.2	−0.016	0.029	−0.010	0.003

use interpolated values of the integrand in that region. The potentials are given in Tables I–IV and may be compared with the results for $\Gamma_\sigma = 620$ MeV given in Tables II and III of L1. It is apparent that cancellation is still very strong between the contributions of graphs with zero, one, or two pion pairs connecting to nucleon lines, especially for $r > 0.6\mu^{-1}$.

The total contribution of σ exchange to nucleon-nucleon central and spin-orbit potentials is shown in Figs. 4(a) and 4(b), respectively, for $\Gamma_\sigma = 620$, 1193, and 2386 MeV, with and without the effect of ghost-pole subtraction for $\Gamma_\sigma = 1193$ MeV. For $\Gamma_\sigma = 620$ MeV there is no ghost-pole subtraction. For $\Gamma_\sigma = 2386$ MeV, a principal-value integration over the $\bar{G}_\sigma(q^2)$ pole in Eqs. (28) and (29) of L1 gives an unphysical long-range behavior.

The result of the ghost-pole subtraction is to decrease the sensitivity to Γ_σ for $\Gamma_\sigma > 625.2$ MeV and to ensure a vanishing, physical asymptotic behavior. An examination of Figs. 21–24 of L1 indicates that the smaller ${}^\Gamma V_c^{\sigma E}$ and ${}^\Gamma V_{so}^{\sigma E}$, and hence the larger Γ_σ, are more consistent with realistic potentials.

ACKNOWLEDGMENT

This work was supported in part through funds provided by the U. S. Department of Energy under Contract No. EY-76-C-02-3069.

[1]E. L. Lomon, Phys. Rev. D 14, 2402 (1976).
[2]Arthur S. Wightman (private communication).
[3]P. J. Redmond, Phys. Rev. 112, 1410 (1958).
[4]M. Gell-Mann and M. Lévy, Nuovo Cimento 16, 705 (1960).
[5]S. Weinberg, Phys. Rev. 177, 2604 (1969).